PHYSICAL REVIEW D **86,** 026003 (2012)

Photoproduction and conductivity in dense holographic QCD

Yan Yan Bu*

State Key Laboratory of Theoretical Physics, Institute of Theoretical Physics, Chinese Academy of Science, Beijing 100190, People's Republic of China

Max-Planck-Institut für Physik (Werner-Heisenberg-Institut) Fhringer Ring 6, 80805 München, Germany

(Received 23 April 2012; published 2 July 2012)

We explore the photoemission rate and conductivity in dense QCD by taking the AdS/CFT methods. Specifically, we take three QCD gravity dual models to do comparative studies: D4/D6 model, noncritical Sakai-Sugimoto model and soft-wall AdS/QCD model. We turn on the time component of flavor U(1) gauge field in the bulk side to model the baryon density in QCD. For all three models, we numerically solve the U(1) fluctuation equation to plot the spectral function and photoemission rate for lightlike momenta as well as the AC conductivity. We find that the results for the former two models are very similar to previous studies while the last one show some differences. The conductivity in the soft-wall model seems to be similar to that of holographic superconductor constructed from five-dimensional bulk gravity, i.e. the pseudogap structure. This should be owing to that the infrared (IR) soft-wall (an effective cutoff near the IR of the geometry) produces a mass gap in the dual field theory, which has imprinting in the conductivity as a pseudogap formation. However, the DC conductivity in our computations is finite while it should be a delta peak in holographic superconductor models. Our results show the importance of dilaton running in affecting physical quantities.

DOI: 10.1103/PhysRevD.86.026003 PACS numbers: 11.25.Tq

I. INTRODUCTION

Data from relativistic heavy ion collision experiments seems to indicate that the QCD plasma, produced during the relativistic heavy ion collision, is strongly coupled and behaves like perfect liquid [1]. This brings nonperturbative investigations of hadronic matter at high temperature and high density, produced in relativistic heavy ion collision experiments, into an urgent stage. The lattice method, used to explore some properties of thermal QCD, is still constrained to extract static quantities of QCD at strongly coupled regime, such as hadron mass spectrum and thermodynamical behavior. What is worse is that when adding finite density or chemical potential to thermal QCD, the lattice calculation usually confronts notorious sign problem. Therefore, improvement in theoretical understanding of strongly coupled quark gluon plasma (sQGP) should not only go beyond traditional perturbative QCD (pQCD) approach but also reveal some properties out of equilibrium, such as transport properties, dispersion relation and high-energy scattering.

AdS/CFT correspondence [2], which is based on string theory or M theory, is a powerful tool in investigating strong coupling regime of gauge field theory and has given us insight into properties of sQGP, see Ref. [3] for an incomplete list of recent reviews. However, it is still a mystery why these calculations based on large N gauge theory, mostly $\mathcal{N} = 4$ supersymmetric Yang-Mills (SYM) theory, can work so well for QCD. Actually, there are some attempts to construct a QCD gravity dual under the framework of gauge/gravity duality in the hope of mimicking behavior of realistic QCD phenomena at low energy or QCD plasma, see Refs. [4–6] for original references.

Photon or dilepton production, which should be an important signal of sQGP and carries some key information of sQGP in the early stage, in $\mathcal{N} = 4$ SYM plasma was discussed in detail both in the strong and weak coupling regime in Ref. [7]. It was found there that the current-current spectral functions in strongly coupled theory exhibit hydrodynamic peaks at small frequency, but otherwise show no peak structure which could be interpreted as well-defined thermal resonances in the high temperature phase. Following this pioneering work, the analysis was soon generalized to D3/D7 and D4/D6 brane systems in Ref. [8], high temperature version of the Sakai-Sugimoto model in Ref. [9], soft-wall AdS/QCD model in Ref. [10], strongly coupled anisotropic plasma in Ref. [11] and $\mathcal{N} = 4$ SYM plasma at large but finite 't Hooft coupling in Ref. [12]. Some references[9,13,14] also studied photoemission rate at finite charge density. All of these works have seen some common features of photoproduction from QCD-like plasma, which suggests that AdS/CFT correspondence can be thought of as a useful tool in describing universal properties of strongly coupling regime of QCD plasma. However, there are some shortcomings of above models. The models based on black D3-brane geometry (or AdS_5 black hole) is conformal and cannot catch the running behavior of strong interaction described by QCD, the quark mass is zero in the Sakai-Sugimoto model, the density in Ref. [14] is from the adjoint sector and should be different from the baryon density. The last drawback is that the models based on 10-dimensional supergravity

*yybu@itp.ac.cn

geometry has the unwanted internal space and results in Kaluza-Klein (KK) modes in the dual QCD (of the same energy scale of hadron spectra), which has no correspondence in QCD phenomena.

Motivated by these studies and shortcomings of these models mentioned above, we in this work carry out a comparative study by taking three different QCD gravity dual models: the D4/D6 system, noncritical Sakai-Sugimoto model and soft-wall model. We will reveal the effect of finite baryon density from the flavor sector on the photoproduction rate and AC conductivity of the dual plasma. We also probe the effect of IR soft-wall, which is essential in describing linear confinement in QCD phenomena. For the photoemission, we find that all the three models give similar results: it is increasing in the low frequency regime when increasing the baryon density; while in the ultraviolet (UV) regime it approaches zero due to the statistical suppression as in blackbody radiation. This indicates that the internal space (in the critical supergravity geometry) nearly has no effect on the physical results we are concerned with here. As to the conductivity of plasma, we find that the soft-wall model gives nontrivial results, in the low density regime (compared to the dimensionless parameter c denoting the IR cutoff) there comes out a gap-like structure. We can understand this as the imprinting of the mass gap formation in the dual gauge theory due to effective IR cutoff triggered by the dilaton suppression in the infrared.

The rest of this work is organized as follows. In Sec. II we concisely introduce our holographic setup and then review the computations of photon production rate and conductivity using the AdS/CFT approach, which can be found in Ref. [7] for more details. Sections III, IV, and V are devoted to numerical computations of the photoproduction and plasma conductivity in all regime of frequency for all the three models. We summarize our work in Sec. VI.

II. HOLOGRAPHIC SETUP AND PHOTOPRODUCTION IN THERMAL FIELD THEORY

A. Formulae for photoproduction and plasma conductivity

Spontaneous photoproduction from medium that is composed of electrically charged particles is a good signal to probe its properties. The spectra of produced photons depend on the details of the system. Moreover, it is expected that the emitted photon from quark gluon plasma (QGP) has little to do with blackbody radiation distribution but may give valuable information about the properties of QGP. However, as mentioned at the beginning of Sec. II, the produced QGP in the relativistic heavy ion collision is perhaps strongly coupled and we therefore need a nonperturbative treatment of calculations of the photoemission from sQGP. This is why AdS/CFT correspondence sets in and plays a more and more important role in studying properties of sQGP. We here follow Ref. [7] to briefly list basic formulae for computing the photoproduction rate and AC conductivity associated with QCD-like plasma.

Consider a thermal system, which can be described by finite temperature quantum field theory. We assume the interaction between the photon and matter takes the electromagnetic current form $eJ_\mu A^\mu$, where J_μ is the electromagnetic current and e is the electromagnetic coupling constant. From thermal field theory [15], the photoproduction rate Γ_γ from a thermal system in equilibrium, to leading order in e, is given by

$$d\Gamma_\gamma = \frac{d^3q}{(2\pi)^3 2\omega} e^2 n_B(\omega) \eta^{\mu\nu} \chi_{\mu\nu}(k)|_{\omega=|\vec{q}|}, \tag{1}$$

where $n_B = 1/(e^{\omega/T} - 1)$ is the Bose-Einstein distribution function, $k^\mu = (\omega, \vec{q})$ is the four-momentum vector, $\eta_{\mu\nu} = (-1, 0, 0, 0)$ denotes the Minkowski metric, and $\chi_{\mu\nu}$ is the spectral function, defined by the following equations,

$$\begin{aligned} \chi_{\mu\nu}(k) &= -2\,\mathrm{Im} G^R_{\mu\nu}(k), \\ G^R_{\mu\nu}(k) &= \int d^4x e^{-ik\cdot x} \langle J_\mu(0) J_\nu(x) \rangle_T \theta(-t). \end{aligned} \tag{2}$$

Here, the symbol $\langle \cdots \rangle_T$ denotes the expectation value taken in the thermal equilibrium state and $x^\mu = (t, \vec{x})$. The AC conductivity can be extracted from the Kubo's formula,

$$\sigma(\omega) = \frac{G^R_{ii}(\omega, \vec{k} = 0)}{i\omega}, \tag{3}$$

where $G^R_{ii}(\omega, \vec{k} = 0)$ denotes spatial component of the retarded Green's function $G^R_{\mu\nu}(\omega, \vec{k} = 0)$.

At nonzero temperature, the Lorentzian invariance of relativistic quantuam field theory is explicitly broken. Fortunately, the unbroken rotational symmetry and gauge invariance allow one to decompose the retarded Green's function $G^R_{\mu\nu}(k)$ into transversal and longitudinal parts [16] as follows,

$$G^R_{\mu\nu}(k) = P^T_{\mu\nu}(k)\Pi^T(k) + P^L_{\mu\nu}(k)\Pi^L(k). \tag{4}$$

The projective operators are defined as

$$\begin{aligned} P^T_{ij}(k) &= \delta_{ij} - \frac{q_i q_j}{|\vec{q}|^2}, \qquad P^T_{0\nu} = 0, \\ P^L_{\mu\nu}(k) &= \eta_{\mu\nu} - \frac{k_\mu k_\nu}{k^2} - P^T_{\mu\nu}(k). \end{aligned} \tag{5}$$

Plugging the above operators into Eq. (4) results in the following form for the trace of the spectral function,

$$\chi^\mu_\mu = -4\,\mathrm{Im}\Pi^T(k) - 2\,\mathrm{Im}\Pi^L(k). \tag{6}$$

Recall that, in this paper we focus on the real photon production and therefore set $\omega = |\vec{q}|$. Then, only the transversal part $\Pi^T(k)$ contributes to the trace of spectral density (because if $\Pi^L(k) \neq 0$, there will be singularity in the

retarded Green's function due to the lightlike momenta chosen for real photon production).

In a short summary, the goal of revealing the photoproduction and AC conductivity of sQGP is reduced to calculations of the retarded Green's function for electromagnetic current J_μ. Under AdS/CFT correspondence, once weakly gauging the flavor U(1) symmetry in the world volume of probe D-brane and treating it as an analogue of the electromagnetic symmetry, our task is further reduced to compute this flavor current-current correlator under the prescription given in Ref. [17].

B. Holographic setup for the QCD gravity dual

The QCD gravity dual in general can be summarized as the following geometric metric with 1 dilaton background ϕ,

$$ds^2 = g_{tt}dt^2 + g_{uu}du^2 + g_{ij}dx^i dx^j + g_S dS^2, \quad (7)$$

where dS^2 denotes the internal space for 10-dimensional supergravity metric. The above metric and dilaton can be sourced by the Einstein-dilaton system. To make the dual QCD-like theory at finite temperature, one can push above geometry to a black hole and identify the Hawking temperature as that of the boundary field theory. To mimic the baryon density, we take the probe D-brane method and turn on background for the time component of the flavor U(1) gauge field, $A_t(u)$. The embedding profile $\chi(u)$ of the probe D-brane and the gauge field configuration $A_t(u)$ can be determined by minimizing the Dirac-Born-Infeld (DBI) action for the probe D-brane. However, here we choose the trivial profile $\chi'(u) = 0$ to simplify our analysis and leave the complicated flavor embedding profile for future publication.

With the above assumptions, the DBI action[1] for the probe Dq-brane is

$$S = -T_q N_f \int d^{q+1}x e^{-\phi}\sqrt{-\det(g + F^0)}, \quad (8)$$

where we set $2\pi l_s^2 = 1$ for brevity, N_f denotes the number of flavor brane, g is the induced metric in the flavor world volume and F^0 is the field strength constructed from A_t. Once the background for the gauge field A_t is worked out, we can fluctuate the system and compute the current-current correlator following the prescription of Ref. [17].

III. D4/D6 MODEL

Intersecting D-brane systems have been widely used to study flavored large N gauge theory at strong coupling, hoping to give some physical intuition to QCD in the strong coupling regime, since the seminal paper [18] and also have produced fruitful results. In this section we also take the intersecting D-brane system as our starting point. To be specific, we choose the D4/D6 model as the QCD gravity dual. This model was first studied in Ref. [4] and revealed many interesting properties for hadron physics in QCD. It is based on D4-brane geometry in type IIA supergravity,

$$ds^2 = \left(\frac{u_0}{R}\right)^{3/2} u^{-3/2}(-f(u)dt^2 + d\vec{x}^2 + dx_4^2) + R^{3/2}u_0^{1/2}u^{-5/2}\frac{du^2}{f(u)} + R^{3/2}u_0^{1/2}u^{-1/2}d\Omega_4^2, \quad (9)$$

with internal space Ω_4 parameterized as

$$d\Omega_4^2 = d\theta^2 + \cos^2\theta d\Omega_2^2 + \sin^2\theta d\xi^2, \quad (10)$$

where the black factor is $f(u) = 1 - u^3$. There is also a background for the dilaton field $e^\phi = g_s(u_0/R)^{3/4}u^{-3/4}$. In our convention for the metric, the black hole horizon is located at $u = 1$ and $u = 0$ denotes the conformal boundary where the dual field theory lives. To avoid a conical singularity in (t, u) plane, the time direction should be periodically identified, i.e., $t \sim t + \beta$ with Hawking temperature $T = 1/\beta = \frac{3}{4\pi}u_0^{1/2}/R^{3/2}$.

The flavor D6-brane extends along $(t, \vec{x}, u, \Omega_2)$ and its embedding profile is specified by $\theta(u)$. As mentioned in Sec. II, here we choose the trivial profile for the flavor sector, i.e., $\theta(u) = 0$ and the induced metric on the flavor world volume takes following form,

$$ds_{\rm ind}^2 = \left(\frac{u_0}{R}\right)^{3/2} u^{-3/2}(-f(u)dt^2 + d\vec{x}^2) + R^{3/2}u_0^{1/2}u^{-5/2}\frac{du^2}{f(u)} + R^{3/2}u_0^{1/2}u^{-1/2}d\Omega_2^2. \quad (11)$$

Plugging the induced metric (11) into Eq. (8) determines the gauge field configuration,

$$\partial_u A_0 = \sqrt{\frac{-d^2 g_{tt}g_{uu}}{g_{xx}^3 g_\Omega^2 e^{-2\phi} + d^2}}, \quad (12)$$

where the integration constant d can be identified as the baryon charge density.

To study the photoproduction, we need perturb the system by including fluctuation of gauge field, $A_M \to A_M + a_M$ where M denotes all the indices in Eq. (11). To quadratic order in gauge field fluctuation a_M, the DBI action can be expanded to the following form [we here omit the background part as in Eq. (8)],

$$S_{\rm fl} = -\frac{N_f T_6}{4}\int d^4x du d\Omega_2 e^{-\phi}\sqrt{-\det(g_{\rm ind} + F^0)}f_{MN}f^{MN} \equiv -\frac{\mathcal{N}'}{4}\int dx^4 du\sqrt{-\mathcal{G}}f_{\mu\nu}f^{\mu\nu}. \quad (13)$$

In the second equality of above equation, we have assumed that the fluctuation a is singlet with respect to internal space Ω_2 and also chosen the components of a along

[1]Here we focus on the U(1) part of the DBI action and there is no Chern-Simons term in our case.

Ω_2 to zero and absorbed the integration over Ω_2 to the prefactor $\mathcal{N}'$. With the SO(3) rotational symmetry, we can take the Fourier ansatz for a_μ of the form

$$a_\mu(t,\vec{x},u)=\int\frac{d^4k}{(2\pi)^4}a_\mu(k,u;d)e^{-i\omega t+\vec{k}\cdot\vec{x}},\quad\text{with}\quad\vec{k}=(q,0,0), \tag{14}$$

where, without loss of generality, the spatial momentum has been chosen to be along x direction. The contraction of indices μ, ν uses the symmetric part G of $(g_{\rm ind}+F^0)^{-1}$ defined as follows,

$$(g_{\rm ind}+F^0)^{-1}=G+J \tag{15}$$

with the diagonal part G given by

$$G^{\mu\nu}=\text{diag}\left(\frac{g_{uu}}{g_{tt}g_{uu}+(\partial_u A_0)^2},\frac{g_{tt}}{g_{tt}g_{uu}+(\partial_u A_0)^2},g^{xx},g^{yy},g^{zz}\right). \tag{16}$$

The equation of motion for the transverse modes, say a_y, is easily worked out by the variational method,

$$\partial_u^2 a_y(k,u;d)+\partial_u\ln(\sqrt{-\mathcal{G}}G^{uu}G^{yy})\partial_u a_y(k,u;d)-\left(\frac{G^{tt}}{G^{uu}}\omega^2+\frac{G^{xx}}{G^{uu}}q^2\right)a_y(k,u;d)=0. \tag{17}$$

In deriving this equation, we choose the radial gauge, $a_u=0$. Substitute Eqs. (12) and (16) into Eq. (17) and simplify by some algebraic manipulations, we obtain the following equation

$$\partial_u^2 a_y(k,u;d)+\left[\frac{f'(u)}{f(u)}+\frac{g'(u)}{2g(u)}\right]\partial_u a_y(k,u;d)+\left[\frac{\tilde{\omega}^2}{uf(u)^2}-\frac{\tilde{q}^2}{uf(u)g(u)}\right]a_y(k,u;d)=0, \tag{18}$$

with dimensionless frequency and momentum defined as

$$\tilde{\omega}=\frac{3}{4\pi T}\omega,\qquad\tilde{q}=\frac{3}{4\pi T}q, \tag{19}$$

and function $g(u)$ given by

$$g(u)=1+\tilde{d}^2u^4,\qquad\tilde{d}=\left(\frac{3}{4\pi T}\right)^2 d. \tag{20}$$

In order to compute the retarded Green's function for operator dual to a_y mode, we use the equation of motion as in Eq. (17) to change the action in Eq. (13) to the following form by integrating by parts,

$$S_{\rm fl}=-\frac{\mathcal{N}'}{2}\int\frac{d^4k}{(2\pi)^4}\times\left\{\sqrt{-\mathcal{G}}G^{uu}G^{yy}a_y(-k,u;d)\partial_u a_y(k,u;d)\right\}\Big|_{u=0}^{u=1}. \tag{21}$$

Then, following the prescription of Ref. [17], the retarded Green's function for the mode a_y is given by

$$G^R_{yy}(k)=\mathcal{N}'\frac{\sqrt{-\mathcal{G}}G^{uu}G^{yy}a_y(-k,u;d)\partial_u a_y(k,u;d)}{a_y(-k,0;d)a_y(k,0;d)}\Big|_{u=0}, \tag{22}$$

with $a_y(k,u;d)$ taking ingoing wave boundary condition at the horizon $u=1$.

Generically, one cannot get analytical solution to Eq. (18) in the whole regime of parameters $\{\tilde{\omega},\tilde{q},\tilde{d}\}$, we then turn to a numerical method to solve it. We begin by presenting the asymptotic behaviors for $a_y(k,u;d)$ near the conformal boundary $u=0$ and horizon $u=1$. Frobenius analysis reveals that, near the horizon,

$$a_y(k,u\sim1;d)\simeq(1-u)^{-i\tilde{\omega}/3}[1+a_y^{(1)}(1-u)+a_y^{(2)}(1-u)^2+a_y^{(3)}(1-u)^3+\cdots], \tag{23}$$

where we have set the scale of $a_y(k,u;d)$ to one given the linearity of Eq. (18) and the minus index $-i\tilde{\omega}/3$ is chosen for ingoing wave boundary condition at the horizon for the purpose of retarded Green's function; near $u=0$,

$$a_y(k,u\sim0;d)\simeq a_y(k,0;d)+ua_y^1(k,0;d)+\cdots. \tag{24}$$

In Eq. (23), these expansion coefficients are uniquely determined in terms of three parameters $\{\tilde{\omega},\tilde{q},\tilde{d}\}$. We will use the expansion near the horizon as the initial conditions and call the Mathematica NDSolve to solve Eq. (18) numerically. The retarded Green's function can be easily read off from the expansion in Eq. (24) and the formula in Eq. (22),

$$G^R(k)=\mathcal{N}\frac{a_y^1(k,0;d)}{a_y(k,0;d)}. \tag{25}$$

Roughly speaking, the factor $\mathcal{N}$ counts the degree of freedom for flavor sector, $\mathcal{N}\sim N_fN_c$. The explicit form of the normalization factor $\mathcal{N}$ will be given in the end of Sec. V. In what follows we list our numerical results as well as some general comments.

In Fig. 1 we plot the trace of the spectral function for real photon production, $\chi^\mu_\mu(q=\omega)/\omega$, weighted by factor $\mathcal{N}$. From different curves, we conclude that the baryon density significantly enlarges the spectral function at low ω/T regime, which is consistent with physical intuition. Concentrating on the $\tilde{d}=0$ curve, we find that for a quite large regime of frequency, the trace of the spectral function $\chi^\mu_\mu(q=\omega)/\omega$ has linear behavior. Analytical computation of spectral function at low/high frequency have been carried out in Refs. [7,9], which is consistent with our numerical result. Once turning on the baryon density, the linear regime in the trace spectral function narrows, which can also be read off from Fig. 2 for the photoemission rate below.

Fig. 2 is for the profile of the photoemission rate $d\Gamma/d\omega$ from QCD-like plasma dual to D4/D6 model at finite baryon density. Explicitly, the photoproduction is enhanced when

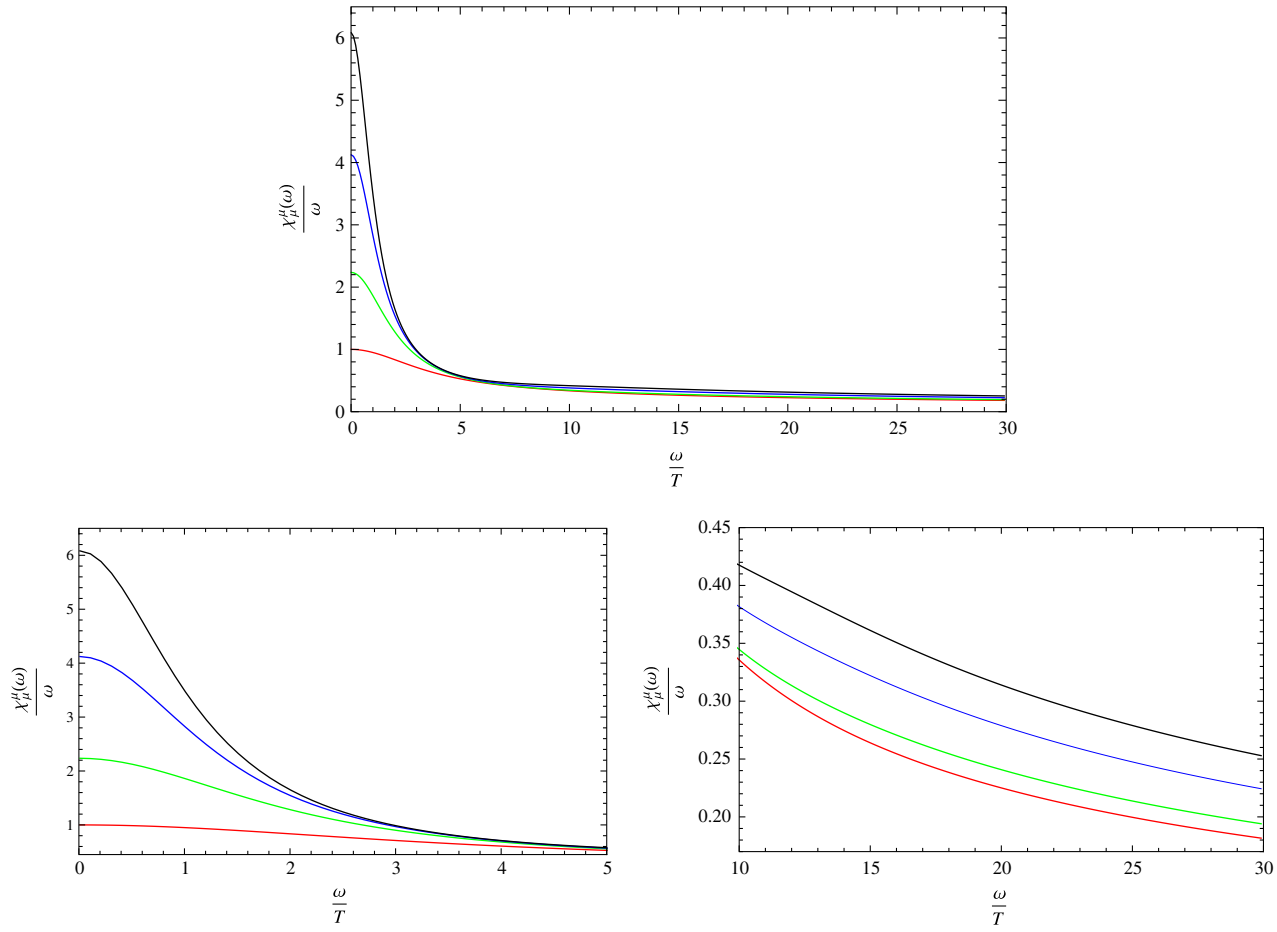

FIG. 1 (color online). D4/D6 model: trace of the spectral function for lightlike momenta divided by frequency, $\eta^{\mu\nu}\chi_{\mu\nu}(q=\omega)/\omega$, in units of $\mathcal{N}$; different curves correspond to different dimensionless baryon density: $\tilde{d}=0$ (red), 2.0 (green), 4.0 (blue), 6.0 (black).

increasing the baryon charge density. Moreover, there is a redshift for the peak frequency ω_p, which maximizes the photoproduction rate, as increasing the baryon charge density. What is consistent with Fig. 1 is that before increasing ω to ω_p, the rate is approximately linearly increasing. The large ω behavior is dominated by the suppression of Bose-Einstein factor. However, the profile for the photoproduction rate is quite different from that of the blackbody radiation spectrum, especially in the intermediate regime of the frequency space. This can also be seen explicitly from plots later in this paper (Figs. 5, 8, 11, and 14). This proves the claim in Ref. [7] that the photoproduction rate from QCD plasma has nothing to do with that of blackbody radiation and is not only due to thermal effect.

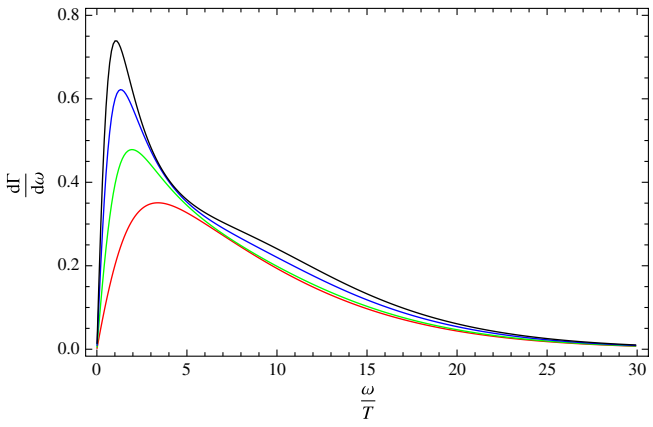

FIG. 2 (color online). D4/D6 model: photoproduction rate $d\Gamma/d\omega$, weighted in units of $\mathcal{N}\frac{e^2}{4\pi}$, at different baryon density corresponding to Fig. 1.

In Fig. 3 we plot the AC conductivity of dense holographic plasma dual to D4/D6 model at different baryon density. We first consider the DC conductivity, corresponding to $\sigma(\omega=0)$. On physical grounds, large baryon density will enhance electrical conduction ability of QCD plasma. This is explicit in our plots in Fig. 3. From the conductivity profiles, we can obtain much information on dense holographic plasma. When the baryon density is very small, corresponding to the red and green curves in Fig. 3, real part of the conductivity is monotonically increasing when walking towards higher frequency regime. However, as the baryon density is large enough, the results are more complicated. In the infrared regime of ω, real part of the conductivity first decreases and then rapidly

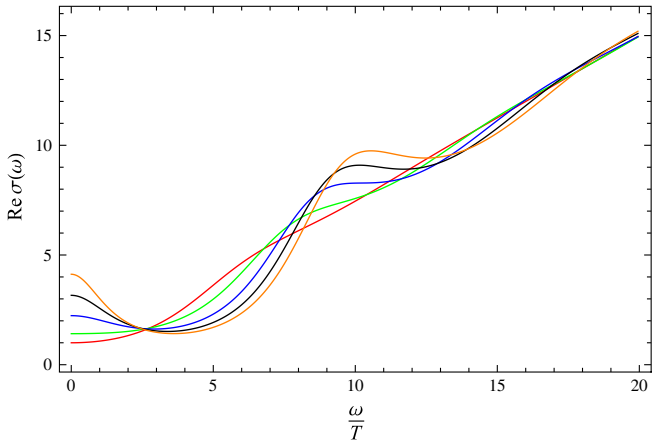

FIG. 3 (color online). D4/D6 model: real part of the AC conductivity corresponding to different baryon density $\tilde{d} = 0.0$ (red), 1.0 (green), 2.0 (blue), 3.0 (black), 4.0 (yellow).

increases to some approximate plateaux. For all of these curves, they have common asymptotic behavior at large ω/T, linear behavior, which is a universal behavior for 4 + 1-dimensional bulk theory, dual to 4-dimensional strongly coupled field theory. This universal behavior has also been revealed in holographic superconductor models in Ref. [19].

In Sec. V, we will consider soft-wall AdS/QCD model and carry out parallel computations as in this section. When the soft-wall cutoff $c = 0$, it reproduces part results of Ref. [7]. Comparing the figures of subsection V A with above ones, we find that they are qualitatively the same. Together with results being stated in Sec. IV, we may conclude that the nonconformal characteristic of supergravity has no significant effect on the physical results like photoproduction rate and plasma conductivity. However, this is not the whole story. Note that the dilaton background in D4/D6 or noncritical Sakai-Sugimoto model is of the type $e^{\phi} \sim u^{\alpha}$ with α some model-dependent constant. This type of dilaton background has no effect in the infrared regime compared to the soft-wall AdS/QCD model. The discussion here also indicates that well-studied top-down approach to QCD-like theory from critical/noncritical supergravity cannot catch some key feature of gauge coupling running in QCD. Therefore, a more realistic QCD gravity dual should be constructed. We will come to this point in later sections.

IV. NONCRITICAL SAKAI-SUGIMOTO MODEL

The other intersecting D-brane system considered in this work is based on AdS_6 black hole solution for supergravity in six-dimensions under the framework of noncritical string theory. One main motivation for introducing noncritical supergravity background into AdS/CFT correspondence is to get rid of the unwanted KK states [20–22], which are always present in critical supergravity and have the same energy scale with QCD hadron spectra. The QCD-like chiral phase transition, flavor quark transport and parton structure function have been discussed in Refs. [23–27] under this framework. The findings in these references indicate that the thermal phase transition and flavor quark transport under noncritical background is nearly the same as those of the Sakai-Sugimoto model. However, the structure function for sQGP has different scaling dependence, as revealed in Ref. [27], on temperature when expressed in terms of the Bjoken variable. Another main difference from the Sakai-Sugimoto model is on the scalar meson spectrum found in Ref. [28]. In what follows we will briefly review the model and follow the conventions of Ref. [26]. The supergravity solution for AdS_6 black hole is

$$ds^2 = \left(\frac{r_0}{R}\right)^2 \frac{1}{u^2}(-f(u)dt^2 + d\vec{x}^2 + dx_4^2) + \left(\frac{R}{u}\right)^2 \frac{du^2}{f(u)}, \quad (26)$$

with the dilaton background and black factor given by

$$e^{\phi} = \frac{2\sqrt{2}}{\sqrt{3}N_c}, \qquad f(u) = 1 - u^5. \quad (27)$$

The quark sector can be introduced in the quenched approximation by adding probe $D4/\overline{D4}$ branes into above supergravity geometry. Here we consider the chiral symmetry restoring phase and the induced metric on the flavor world volume is

$$ds^2_{\text{ind}} = \left(\frac{r_0}{R}\right)^2 \frac{1}{u^2}(-f(u)dt^2 + d\vec{x}^2) + \left(\frac{R}{u}\right)^2 \frac{du^2}{f(u)}. \quad (28)$$

To make the holographic plasma to be dense medium, as in D4/D6 model we consider the time component of flavor U(1) gauge field $A_0(u)$. Its configuration is of the form

$$\partial_u A_0 = \sqrt{\frac{-d^2 g_{tt} g_{uu}}{g_{xx}^3 + d^2}}, \quad (29)$$

where d is the baryon charge density. For photoproduction and conductivity, we study perturbation of the system and compute the current-current correlator. Following similar procedure as in D4/D6 model, the equation of motion for the fluctuation mode $a_y(k, u; d)$ is given by

$$\partial_u^2 a_y(k,u;d) + \left[\frac{f'(u)}{f(u)} - \frac{1}{u} + \frac{g'(u)}{2g(u)}\right]\partial_u a_y(k,u;d) + \left[\frac{\tilde{\omega}^2}{f(u)^2} - \frac{\tilde{q}^2}{f(u)g(u)}\right] a_y(k,u;d) = 0, \quad (30)$$

with dimensionless frequency and momentum defined as

$$\tilde{\omega} = \frac{5}{4\pi T}\omega, \qquad \tilde{q} = \frac{5}{4\pi T} q, \quad (31)$$

and function $g(u)$ given by

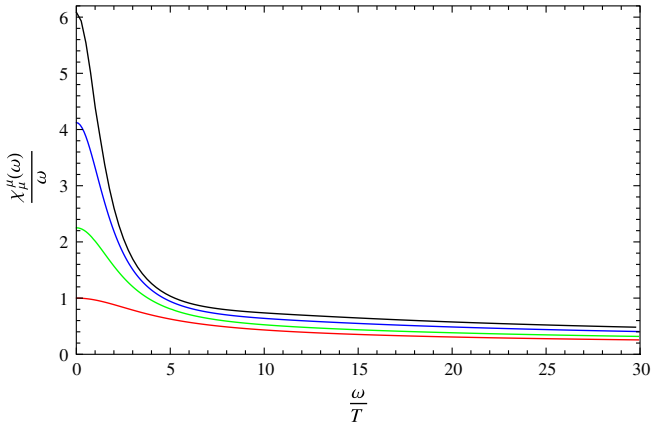

FIG. 4 (color online). Noncritical Sakai-Sugimoto model: trace of the spectral function for lightlike momenta divided by frequency, $\chi^{\mu}_{\mu}(q = \omega)/\omega$; different curves correspond to different dimensionless baryon density: $\tilde{d} = 0$ (red), 2.0 (green), 4.0 (blue), 6.0 (black).

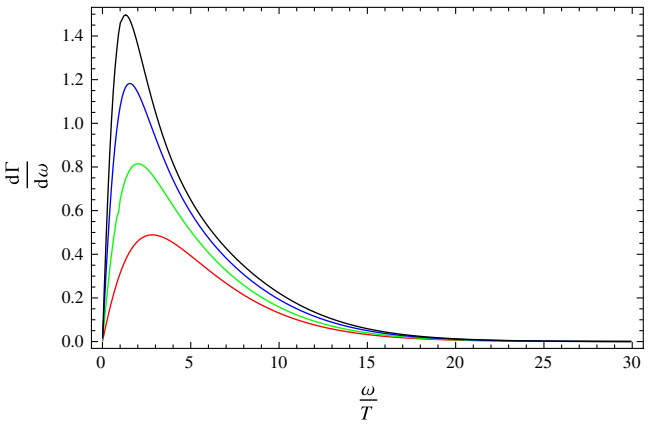

FIG. 5 (color online). Noncritical Sakai-Sugimoto model: photoproduction rate $d\Gamma/d\omega$ at different dimensionless baryon density corresponding to plots in Fig. 4.

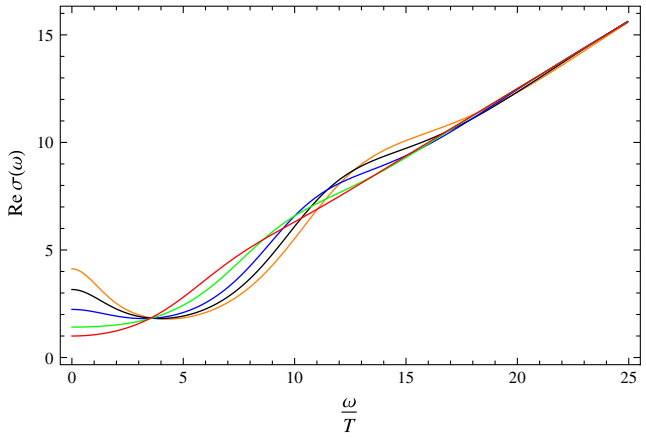

FIG. 6 (color online). Noncritical Sakai-Sugimoto model: real part of the AC conductivity corresponding to different baryon density: $\tilde{d} = 0.0$ (red), 1.0 (green), 2.0 (blue), 3.0 (black), 4.0 (orange).

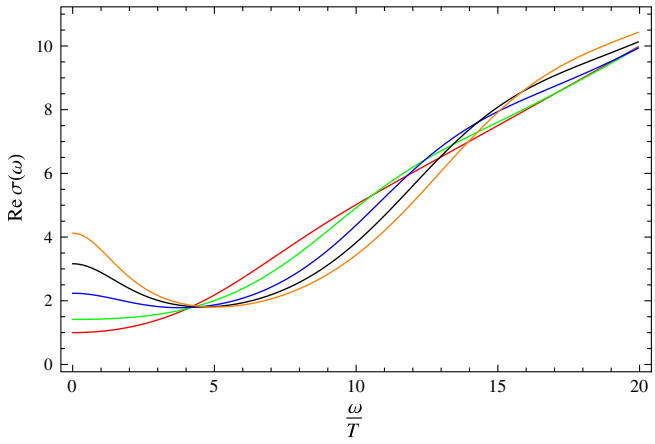

FIG. 7 (color online). Super-Yang-Mills plasma: real part of the AC conductivity corresponding to different baryon density: $\tilde{d} = 0.0$ (red), 1.0 (green), 2.0 (blue), 3.0 (black), 4.0 (orange).

$$g(u) = 1 + \tilde{d}^2 u^6, \qquad \tilde{d} = \left(\frac{5}{4\pi T}\right)^3 d. \tag{32}$$

It is clear that this equation is basically the same as Eq. (18). It is therefore expected that the associated results in this noncritical supergravity are also similar to those of Sec. III and this is actually what we find in our work. Through Frobenius analysis, we can obtain similar asymptotic behavior for the fluctuation mode $a_y(k, u; d)$ as in Eqs. (23) and (24).

Our numerical results are stated in the following several figures. In Fig. 4, we plot the trace of the spectral function for lightlike momenta, $\chi^{\mu}_{\mu}(q = \omega)/\omega$. Figure 5 is for the plot of the photoemission rate $d\Gamma/d\omega$ from QCD-like plasma and Fig. 6 is real part of the AC conductivity of dense holographic plasma described by noncritical Sakai-Sugimoto model. As mentioned at the end of Sec. III, the associated results presented here are basically the same as those of D4/D6 model. However, there is also one small difference from D4/D6 model on the conductivity. Clearly, there is no plateaux here, which is not present in Fig. 7 for conductivity of SYM plasma, either. This should be thought of as the effect of nonconformality of the supergravity background for D4-brane.

V. SOFT-WALL ADS/QCD MODEL

The last model investigated in our work is the so-called soft-wall AdS/QCD model, which is popular in producing some interesting properties in hadron physics. This model takes the AdS_5 metric as the dual geometry and introduces the flavor matter into this background [5],

$$S \sim \int d^5x e^{-\phi}\sqrt{-g}\left\{-|DX|^2 + 3|X|^2 - \frac{1}{4g_5^2}(F_L^2 + F_R^2)\right\}, \tag{33}$$

where the meaning of different fields in above action can be found in Ref. [5]. The dilaton profile is $\phi = cu$ with dimensionless parameter c given by

$$c = \frac{\Lambda_{\rm IR}^2}{(\pi T)^2}, \tag{34}$$

where $\Lambda_{\rm IR}$ is the infrared scale below which our physics is cut off. Roughly speaking, $\Lambda_{\rm IR}$ can be thought of as the energy scale of hadron spectra. We straightforwardly extend this model to black hole case,

$$ds^2 = \frac{(\pi {\rm TR})^2}{u}(-f(u)dt^2 + d\vec{x}^2) + \frac{R^2}{4u^2 f(u)}du^2, \tag{35}$$

where T is the Hawking temperature of AdS_5 black hole and the black factor $f(u) = 1 - u^2$.

To model the baryon density in this model, we follow Secs. III and IV to study Abelian DBI action as in Eq. (8) with metric in Eq. (35) and turn on the time component of the flavor gauge field. The gauge field configuration is solution to the following equation

$$\partial_u A_0 = \sqrt{\frac{-d^2 g_{tt} g_{uu}}{g_{xx}^3 e^{-2\phi} + d^2}}, \tag{36}$$

with d the baryon charge density. Following the same procedure as in previous two sections, we can easily work out equation of motion for the fluctuation mode $a_y(k, u; d)$,

$$\partial_u^2 a_y(k,u;d) + \left[\frac{f'(u)}{f(u)} - c + \frac{g'(u)}{2g(u)}\right]\partial_u a_y(k,u;d) + \left[\frac{\tilde{\omega}^2}{uf(u)^2} - \frac{\tilde{q}^2}{uf(u)g(u)}\right]a_y(k,u;d) = 0, \tag{37}$$

with dimensionless frequency and momentum defined as

$$\tilde{\omega} = \frac{1}{2\pi T}\omega, \qquad \tilde{q} = \frac{1}{2\pi T}q, \tag{38}$$

and function $g(u)$ given by

$$g(u) = 1 + \tilde{d}^2 e^{2cu} u^3, \qquad \tilde{d} = \left(\frac{d}{\pi T}\right)^3. \tag{39}$$

To produce the photoproduction and conductivity, one has to numerically solve Eq. (37) for generic frequency $\tilde{\omega} = \tilde{q}$. The method is same as that of Sec. III and we directly present our results in the subsequent two subsections.

A. Reproducing associated results in SYM plasm: $c=0$

In this subsection we consider the $c = 0$ case, which is same as SYM plasma well-studied in Ref. [7]. However, in this work we include the baryon charge density.[2] In Fig. 8 we plot the trace of the spectral function for lightlike momenta, $\chi^\mu_\mu(q = \omega)/\omega$, at different baryon densities. Figure 9 is for the photoemission rate $d\Gamma/d\omega$ at baryon density corresponding to that of Fig. 8. The AC conductivity of SYM plasma at different baryon density is plotted in Fig. 7. Comparing to the corresponding figures shown in Sec. IV, we find that the results under these two models are basically the same. In actual fact, this should be the case as the supergravity background for these two models are similar. Concentrating on the profile of the AC conductivity, we once again see that there is no plateaux in

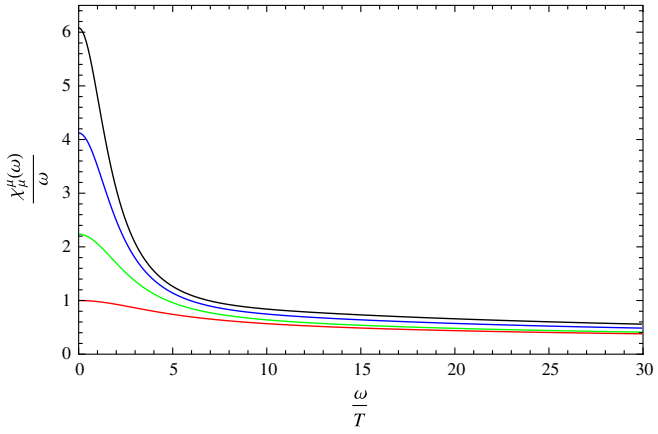

FIG. 8 (color online). Super-Yang-Mills plasma: trace of the spectral function for lightlike momenta divided by frequency, $\chi^\mu_\mu(q = \omega)/\omega$; different curves correspond to different dimensionless baryon density: $\tilde{d} = 0$ (red), 2.0 (green), 4.0 (blue), 6.0 (black).

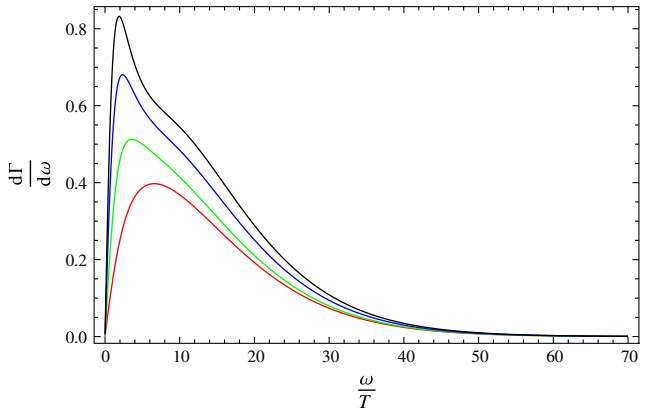

FIG. 9 (color online). Super-Yang-Mills plasma: photoproduction rate $d\Gamma/d\omega$ at different dimensionless baryon density $\tilde{d} =$ 0.0 (red), 2.0 (green), 4.0 (blue), 6.0 (black).

[2]Note in this work we introduce the baryon charge density using nonlinear DBI action and therefore takes into account of nonlinear effect, which is different from R-charge AdS black hole studied in Ref, [14].

intermediate regime of frequency, compared to that of the D4/D6 model. This should be attributed to effect of the dilaton running characteristic of supergravity background. Our results are quite different from those of Ref. [14] which takes the RN-AdS black hole geometry as the gravity dual of QCD and embeds the baryon charge density in the black hole charge.

B. Soft-wall as an effective infrared cutoff: $c \neq 0$

The results in this subsection compose another main part of our work. Our numerical results are listed in Figs. 10–12 for the trace of the spectral function at lightlike momenta $\chi^{\mu}_{\mu}(q = \omega)/\omega$, photoproduction rate $d\Gamma/d\omega$ and real part of the AC conductivity $\mathrm{Re}\sigma(\omega)$, respectively. We choose the cutoff parameter $c = 3$ in these plots and the dimensionless baryon charge density $\tilde{d}$ is same as that of previous plots. Before some discussions, we should note that here

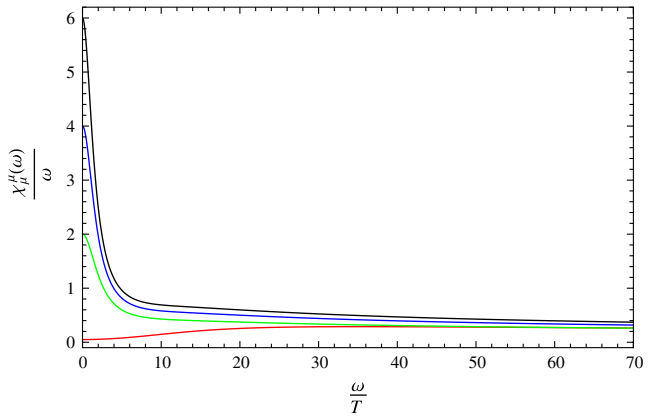

FIG. 10 (color online). Soft-wall model ($c = 3$): trace of the spectral function for lightlike momenta divided by frequency, $\chi^{\mu}_{\mu}(q = \omega)/\omega$; different curves correspond to different dimensionless baryon density: $\tilde{d} = 0.0$ (red), 2.0 (green), 4.0 (blue), 6.0 (black).

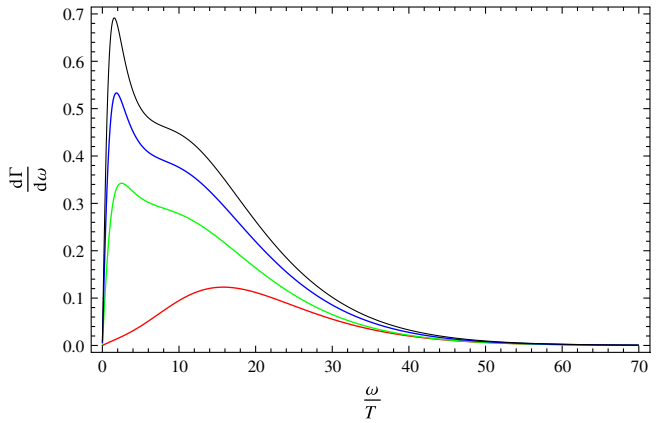

FIG. 11 (color online). Soft-wall model ($c = 3$): photoproduction rate $d\Gamma/d\omega$ at different dimensionless baryon density corresponding to plots in Fig. 10.

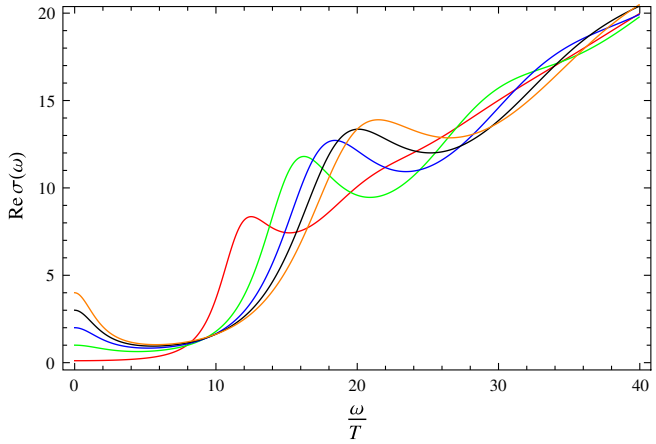

FIG. 12 (color online). Soft-wall model ($c = 3$): real part of the AC conductivity corresponding to different baryon density: $\tilde{d} = 0.0$ (red), 1.0 (green), 2.0 (blue), 3.0 (black), 4.0 (orange).

we scan over the frequency parameter $\tilde{\omega}$ during numerical computations and did not probe the effect of very large baryon density on physical results, which has been simply discussed in Ref. [9]. Therefore, we can expect to find some striking features only in the small frequency regime (infrared regime) of our plots and the asymptotic behavior (ultraviolet regime of frequency) should be similar to previous conclusions, which have been investigated in detail using analytical approximation. Therefore, our discussions will be concentrated on the small frequency regime. Note that in Figs. 10–12 the density $\tilde{d}$ is chosen to be quite large compared to the cutoff parameter $c = 3$. Given this fact, some essential effect will be hidden due to density effect. Therefore in Figs. 13–15 we plot the same quantities but for quite small $\tilde{d}$ variable.

In what follows we will give some comments on these figures. First, consider Fig. 10 for the trace of the spectral

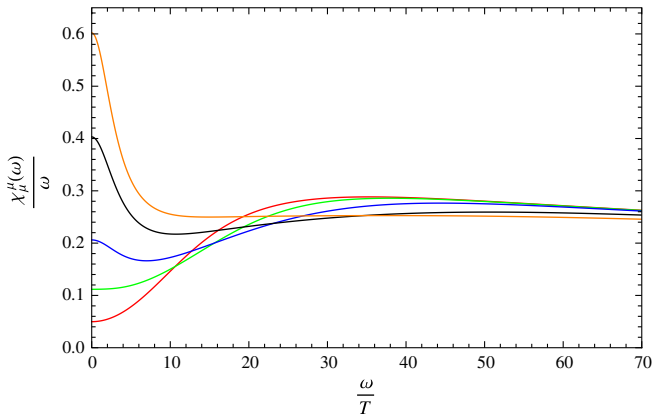

FIG. 13 (color online). Soft-wall model ($c = 3$): trace of the spectral function for lightlike momenta divided by frequency, $\chi^{\mu}_{\mu}(q = \omega)/\omega$; different curves correspond to different dimensionless baryon density: $\tilde{d} = 0.0$ (red), 0.1 (green), 0.2 (blue), 0.4 (black), 0.6 (orange).

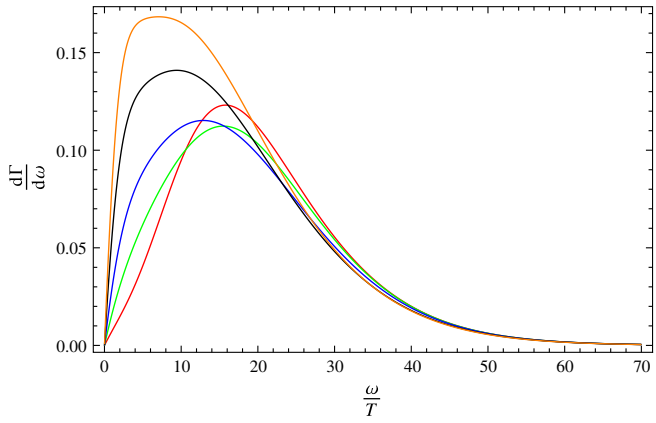

FIG. 14 (color online). Soft-wall model ($c = 3$): photoproduction rate $d\Gamma/d\omega$ at different dimensionless baryon density corresponding to plots in Fig. 13.

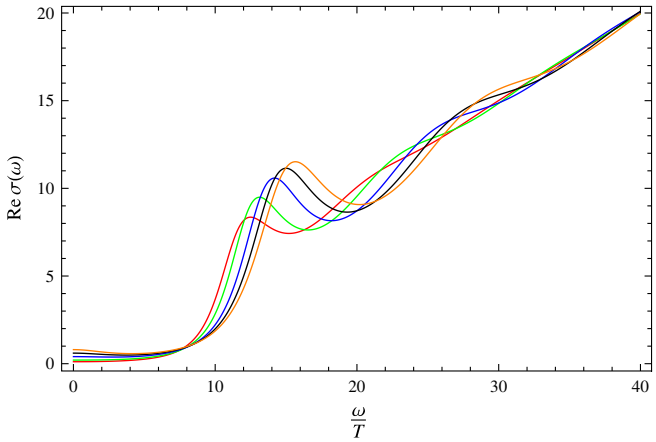

FIG. 15 (color online). Soft-wall model ($c = 3$): real part of the AC conductivity corresponding to different baryon density: $\tilde{d} = 0.1$ (red), 0.2 (green), 0.4 (blue), 0.6 (black), 0.8 (orange).

function at lightlike momenta. We find that the presence of an IR cutoff greatly changes the final results. When dimensionless charge density $\tilde{d}$ is quite small (corresponding to the red curve in Fig. 10, red and green curves in Fig. 13), the spectral function first raises to some value and then decreases very slowly. When the baryon density is large enough, the effect of IR cutoff has been weakened, even erased, and the profile for the trace of the spectral function goes back to those of previous sections. The figures for the photoemission rate are basically same as previous results except that peak value of first curve (the red curve) exceeds the second one (the green curve) as seen in Fig. 13. As in the case of the trace of the spectral function, once the baryon charge density is large enough, see Fig. 11, these curves go back to those of previous sections.

Real part of the AC conductivity shown in Fig. 15 is quite different from previous results. Surprisingly, it looks like that of holographic superconductor model in four-dimensional boundary theory [19], especially when the charge density $\tilde{d}$ is quite small compared to the cutoff parameter c, which can be easily seen in Fig. 15. The most bright feature in our plot is the pseudogap formation in the infrared regime of frequency space. However, we should keep in mind that the gap-like formation here is quite different than that of holographic superconductor model. More specifically, in our work there is no spontaneous symmetry, which does happen in holographic superconductor models and is directly responsible for the gap structure formation in the superconducting conductivity. Another main difference between them is that our result for the DC conductivity is finite while it is a delta peak in holographic superconductor model. The appearance of pseudogap in the infrared can be seen as the imprinting of dilaton soft-wall. Because of the effective cutoff in the infrared of field theory, the approximate plateaux in intermediate regime of frequency are now replaced by metastable valleys which appear at $\tilde{\omega} = 15$–20 in Fig. 15. Combining these results with those of previous sections, we conclude that the dilaton running can have important effect on physical results uncovered here, like the photoemission and conductivity.

Before concluding this work, we give the expression for the normalization factor $\mathcal{N}$, which has been ignored in previous representations. As claimed in Sec. III, this factor counts the flavor degree of freedom and is therefore proportional to $N_f N_c$. Moreover, it also has temperature dependence T^2,

$$\mathcal{N} = \gamma N_f N_c T^2, \tag{40}$$

with γ a model dependent constant

$$\gamma = \begin{cases} \frac{1}{9\pi^2}, & \text{D4/D6 model,} \\ \frac{3}{10\sqrt{5}}, & \text{Noncritical Sakai} - \text{Sugimoto model,} \\ \frac{1}{2\pi}, & \text{Soft} - \text{wall model.} \end{cases} \tag{41}$$

VI. SUMMARY AND DISCUSSIONS

In this work we took three holographic QCD models to study one important signal of sQGP, i.e., the photoemission rate from QCD-like plasma at finite baryon density. Via computations and plots of these physical quantities, we found that the dilaton running can have some effect on this signal especially in the infrared regime of photon frequency. In particular, the more realistic soft-wall AdS/QCD model predicts a pseudogap formation in the profile of AC conductivity. However, the gap-like structure found here should be distinguished from that of holographic superconductor model. These results indicate that running of the gauge coupling constant of QCD-like theory, even at

the infrared regime, can be neglected and may have imprinting in the final results for photoproduction and conductivity. Actually, one realistic AdS/QCD model, which mainly takes into account gauge coupling running, from Einstein-Dilaton system has been established and explored for the purpose of hadron physics in Ref. [6]. We expect to carry out similar computations in this model to reveal some universal characteristics of more realistic AdS/QCD models in the near future.

ACKNOWLEDGMENTS

The author would like to thank Johanna Erdmenger for her encouragement and inspiration as well as some good suggestions during this project. It is my great pleasure to thank the referee for her or his valuable comments on some points in this paper as well as claiming some inappropriate conclusions in the first version of this paper. This work was supported by the MPS-CAS Doctoral Training program.

[1] E. Shuryak, Prog. Part. Nucl. Phys. **53**, 273 (2004); E. V. Shuryak, in Proceedings of Continuous Advances in QCD, University of Minnesota, 2006 (unpublished).
[2] J. M. Maldacena, Adv. Theor. Math. Phys. **2**, 231 (1998).
[3] J. Erdmenger, N. Evans, I. Kirsch, and E. Threlfall, Eur. Phys. J. A **35**, 81 (2008); R. C. Myers and S. E. Vazquez, Classical Quantum Gravity **25**, 114008 (2008); E. Iancu, Acta Phys. Pol. B **39**, 3213 (2008); S. S. Gubser and A. Karch, Annu. Rev. Nucl. Part. Sci. **59**, 145 (2009); U. Gursoy, Mod. Phys. Lett. A **23**, 3349 (2008); R. A. Janik, Lect. Notes Phys. **828**, 147 (2011); J. Casalderrey-Solana, H. Liu, D. Mateos, K. Rajagopal, and U. A. Wiedemann, arXiv:1101.0618; A. Karch, in Proceedings of the 19th Particles and Nuclei International Conference (PANIC11), Cambridge, Massachussetts, 2011 (unpublished).
[4] M. Kruczenski, D. Mateos, R. C. Myers, and D. J. Winters, J. High Energy Phys. 05 (2004) 041; T. Sakai and S. Sugimoto, Prog. Theor. Phys. **113**, 843 (2005); J. Erlich, E. Katz, D. T. Son, and M. A. Stephanov, Phys. Rev. Lett. **95**, 261602 (2005); L. Da Rold and A. Pomarol, Nucl. Phys. **B721**, 79 (2005).
[5] A. Karch, E. Katz, D. T. Son, and M. A. Stephanov, Phys. Rev. D **74**, 015005 (2006).
[6] U. Gursoy and E. Kiritsis, J. High Energy Phys. 02 (2008) 032.U. Gursoy, E. Kiritsis, and F. Nitti, *ibid.*02 (2008) 019.
[7] S. Caron-Huot, P. Kovtun, G. Moore, A. Starinets, and L. G. Yaffe, J. High Energy Phys. 12 (2006) 015.
[8] D. Mateos and L. Patino, J. High Energy Phys. 11 (2007) 025.
[9] A. Parnachev and D. A. Sahakyan, Nucl. Phys. **B768**, 177 (2007).
[10] A. Nata Atmaja and K. Schalm, J. High Energy Phys. 08 (2010) 124.
[11] A. Rebhan and D. Steineder, J. High Energy Phys. 08 (2011) 153.
[12] B. Hassanain and M. Schvellinger, Phys. Rev. D **85**, 086007 (2012).
[13] J. Mas, J. P. Shock, J. Tarrio, and D. Zoakos, J. High Energy Phys. 09 (2008) 009.
[14] K. Jo and S.-J. Sin, Phys. Rev. D **83**, 026004 (2011).
[15] M. Le Bellac, *Thermal Field Theory* (Cambridge University Press, Cambridge, England, 1996).
[16] P. K. Kovtun and A. O. Starinets, Phys. Rev. D **72**, 086009 (2005).
[17] D. T. Son and A. O. Starinets, J. High Energy Phys. 09 (2002) 042.
[18] A. Karch and E. Katz, J. High Energy Phys. 06 (2002) 043.
[19] M. Ammon, J. Erdmenger, M. Kaminski, and P. Kerner, Phys. Lett. B **680**, 516 (2009); J. High Energy Phys. 10 (2009) 067; P. Basu, J. He, A. Mukherjee, and H.-H. Shieh, *ibid.*11 (2009) 070; K. Peeters, J. Powell, and M. Zamaklar, *ibid.*09 (2009) 101.
[20] S. Kuperstein and J. Sonnenschein, J. High Energy Phys. 07 (2004) 049.
[21] S. Kuperstein and J. Sonnenschein, J. High Energy Phys. 11 (2004) 026.
[22] F. Bigazzi, R. Casero, A. L. Cotrone, E. Kiritsis, and A. Paredes, J. High Energy Phys. 10 (2005) 012.
[23] V. Mazo and J. Sonnenschein, J. High Energy Phys. 06 (2008) 091.
[24] S.-l. Cui, Y.-h. Gao, Y. Seo, S.-j. Sin, and W.-s. Xu, Phys. Rev. D **81**, 066001 (2010).
[25] S.-l. Cui, Y.-h. Gao, and W.-s. Xu, Phys. Rev. D **81**, 026008 (2010).
[26] Y. Y. Bu and J. M. Yang, Nucl. Phys. **B855**, 388 (2012).
[27] Y. Y. Bu and J. M. Yang, Phys. Rev. D **84**, 106004 (2011).
[28] O. Mintakevich and J. Sonnenschein, J. High Energy Phys. 08 (2008) 082.